Title

Ontogenetic changes in cutaneous and branchial ionocytes and morphology in yellowfin tuna (Thunnus albacares) larvae.

Journal

Journal of comparative physiology. B, Biochemical, systemic, and environmental physiology, 189(1)

ISSN

0174-1578

Authors

Kwan, Garfield T

Wexler, Jeanne B

Wegner, Nicholas C

et al.

Publication Date

2019-02-01

DOI

10.1007/s00360-018-1187-9

Peer reviewed

Journal of Comparative Physiology B (2019) 189:81–95
https://doi.org/10.1007/s00360-018-1187-9

ORIGINAL PAPER

Ontogenetic changes in cutaneous and branchial ionocytes and morphology in yellowfin tuna (*Thunnus albacares*) larvae

Garfield T. Kwan[1] · Jeanne B. Wexler[2] · Nicholas C. Wegner[3] · Martin Tresguerres[1]

Received: 9 March 2018 / Revised: 1 October 2018 / Accepted: 16 October 2018 / Published online: 24 October 2018

Abstract

The development of osmoregulatory and gas exchange organs was studied in larval yellowfin tuna (*Thunnus albacares*) from 2 to 25 days post-hatching (2.9–24.5 mm standard length, SL). Cutaneous and branchial ionocytes were identified using Na^+/K^+-ATPase immunostaining and scanning electron microscopy. Cutaneous ionocyte abundance significantly increased with SL, but a reduction in ionocyte size and density resulted in a significant decrease in relative ionocyte area. Cutaneous ionocytes in preflexion larvae had a wide apical opening with extended microvilli; however, microvilli retracted into an apical pit from flexion onward. Lamellae in the gill and pseudobranch were first detected ~ 3.3 mm SL. Ionocytes were always present on the gill arch, first appeared in the filaments and lamellae of the pseudobranch at 3.4 mm SL, and later in gill filaments at 4.2 mm SL, but were never observed in the gill lamellae. Unlike the cutaneous ionocytes, gill and pseudobranch ionocytes had a wide apical opening with extended microvilli throughout larval development. The interlamellar fusion, a specialized gill structure binding the lamellae of ram-ventilating fish, began forming by ~ 24.5 mm SL and contained ionocytes, a localization never before reported. Ionocytes were retained on the lamellar fusions and also found on the filament fusions of larger sub-adult yellowfin tuna; however, sub-adult gill ionocytes had apical pits. These results indicate a shift in gas exchange and NaCl secretion from the skin to branchial organs around the flexion stage, and reveal novel aspects of ionocyte localization and morphology in ram-ventilating fishes.

Keywords Chloride cell · Osmoregulation · Fish larvae · Mitochondrion-rich cell · Ionocyte · Gill morphology

Introduction

Marine teleost fish are hypoosmotic and hypoionic compared to seawater, and actively maintain the NaCl concentration in their blood plasma and extracellular fluids ~ 60% lower than seawater (reviewed in Evans et al. 2005). In adult fish, the resulting diffusive NaCl gain and water loss are counteracted by water absorption in the intestine and active NaCl excretion by specialized gill cells called ionocytes (formerly known as chloride cells or mitochondrion-rich cells) (Marshall and Nishioka 1980; Zadunaisky 1996; reviewed in; Evans et al. 2005). NaCl excretion against the electrochemical gradient is powered by highly abundant Na^+/K^+-ATPases (NKA) located in the highly infolded basolateral membrane of ionocytes, working in concert with basolateral $Na^+/K^+/Cl^-$ co-transporters and apical Cl^- channels (reviewed in Hirose et al. 2003; Evans et al. 2005). Osmoregulation in adult marine teleosts has been thoroughly studied from the whole animal to the molecular level (Evans et al. 1999, 2005; Evans 2002, 2008). It is clear that larval marine

Communicated by G. Heldmaier.

Electronic supplementary material The online version of this article (https://doi.org/10.1007/s00360-018-1187-9) contains supplementary material, which is available to authorized users.

✉ Jeanne B. Wexler
jwexler@iattc.org

✉ Nicholas C. Wegner
nick.wegner@noaa.gov

✉ Martin Tresguerres
mtresguerres@ucsd.edu

[1] Marine Biology Research Division, Scripps Institution of Oceanography, University of California San Diego, 9500 Gilman Drive, La Jolla, CA 92093, USA

[2] Inter-American Tropical Tuna Commission, 8901 La Jolla Shores Drive, La Jolla, CA 92037, USA

[3] Fisheries Resources Division, Southwest Fisheries Science Center, NOAA Fisheries, 8901 La Jolla Shores Drive, La Jolla, CA 92037, USA

teleosts also hypo-osmoregulate their internal fluids (Alderdice 1988; Varsamos et al. 2005), and that NaCl excretion initially takes place across the skin and shifts to the gills when these develop (e.g., Roberts et al. 1973; Hiroi et al. 1998; Katoh et al. 2000; Varsamos et al. 2001; Bodinier et al. 2010). However, many unknowns remain including potential species-specific timing of the shift from skin to gill osmoregulation, the role of the pseudobranch, and the relationship between osmoregulation and gas exchange.

Cutaneous ionocytes in fish larvae were first detected in marine European plaice (*Pleuronectes platessa*) by silver nitrate staining (Shelbourne 1957). Currently, cutaneous ionocytes in fish larvae are usually identified based on their high NKA abundance using immunohistochemical techniques (van der Heijden et al. 1999; Katoh et al. 2000; Varsamos et al. 2002a). At hatching, ionocytes are present throughout the yolk sac and the skin (Holliday 1969; Alderdice 1988; Schreiber 2001; reviewed in; Varsamos et al. 2005). As the fish develops, ionocyte density decreases in the skin and progressively increases at the interlamellar space on the gill filaments (Ayson et al. 1994; Hiroi et al. 1998, 1999; Varsamos et al. 2002a). By the time fish become juveniles, the bulk of NaCl excretion takes place across the gills, with cutaneous ionocytes altogether disappearing in some species as adults (Whitear 1970). This shift in ionocyte distribution is intrinsically related to the reduction in surface to volume ratio that takes place as an organism grows. In smaller larvae with a relatively large surface area to volume ratio, gas exchange and ion transport can take place at adequate rates across the skin (c.f. Goss et al. 1994; Perry and Goss 1994; Varsamos et al. 2002a; Katoh et al. 2003). As larvae grow larger, their surface area to volume ratio decreases, the diffusion distance between capillaries and the surrounding water increases, and developing skin scales and mucus further obstruct diffusion. However, branchial structures (gills and in some cases the pseudobranch) develop and increase the total surface area—providing additional respiratory and osmoregulation capacity to keep up with increased total metabolic rate (reviewed in Rombough 2007).

Several studies have thus examined the transition of osmoregulatory function from the skin to the gills during larval development (Ayson et al. 1994; Hiroi et al. 1998, 1999; Varsamos et al. 2002a). However, little is known about this transition in highly active fishes, such as tunas (family Scombridae) and billfishes (families Istiophoridae and Xiphiidae), which support multibillion dollar fisheries worldwide and differ from most other fishes in their exceptionally high energetic demands and adaptations for ram ventilation. Specifically, tunas, billfishes, and their relatives have significantly larger gill surface areas (Muir and Hughes 1969; Palzenberger and Pohla 1992; Wegner et al. 2010) and thinner lamellae (Muir 1970; Muir and Brown 1971; Olson et al. 2003; Wegner et al. 2006) than most other fishes to optimize respiratory gas exchange and meet their high metabolic rates. While advantageous for enhancing O_2 uptake, additional gill surface area and decreased diffusion distances should increase NaCl diffusive gain, potentially requiring additional NaCl-excreting ionocytes to maintain ionic balance. In addition, while the majority of fish species utilize muscular pumping of the buccal and opercular chambers to ventilate the gills, tunas and other active fish species utilize ram ventilation to drive water into their branchial chambers through fast forward swimming (Brown and Muir 1970; Stevens 1972; Roberts 1975; Stevens and Lightfoot 1986; Wegner et al. 2012, 2013). To prevent gill filaments and lamellae from collapsing under high water flow, some ram ventilators including tunas, bonitos, and billfishes have developed specialized structures that bind together adjacent lamellae (interlamellar and lamellar fusions) and or adjacent filaments (filament fusions) to provide added gill rigidity (Muir and Kendall 1968; Wegner et al. 2006, 2013).

This study thus examines the larval development of osmorespiratory functional morphology in the yellowfin tuna (*Thunnus albacares*, Bonnaterre, 1788), a highly active and ram-ventilating species. The yellowfin tuna spawns in tropical and subtropical oceans worldwide (Schaefer 2001), and supports multinational sport and commercial fishery activities worth $15 billion USD in 2014 (Galland et al. 2016). Yellowfin tuna larvae are usually found within the upper mixed layer of warm waters predominantly between 20 and 30 m and as deep as 50 m (Leis et al. 1991; Boehlert et al. 1992; Boehlert and Mundy 1994), where they are exposed to variable ocean conditions that can affect survival. Several research facilities and aquaculture programs worldwide have supported studies on the early developmental stages of yellowfin tuna, including larval morphology, food selection, age validation, and growth rates (Ambrose 1996; Kaji et al. 1999; Margulies et al. 2001, 2007, 2016; Wexler et al. 2001, 2003, 2007). The objectives of the present study were to investigate the appearance of gas exchange and osmoregulatory structures during larval yellowfin tuna development.

Methods

Larval rearing conditions

A developmental series of yellowfin tuna larvae from 2.9 to 24.5 mm standard length (SL), corresponding to 2–25 days post-hatching (dph), were raised from fertilized eggs collected from a broodstock population of yellowfin tuna that spawn naturally and nearly daily in a land-based tank at the Inter-American Tropical Tuna Commission's Achotines Laboratory in Panama (Wexler et al. 2003; Margulies et al. 2007). Yellowfin tuna eggs and larvae were raised in a flow-through, filtered

seawater system with pH = 8.08 ± 0.03 (mean ± standard error of the mean), temperature = 28.30 ± 0.07 °C, dissolved O_2 = 6.08 ± 0.05 mg/L, and salinity = 33.24 ± 0.06 ppt (Supplementary material 1). Dissolved O_2 levels declined slightly as larval metabolic activity and development increased but were always above 5.5 mg/L, which is within the optimum range for normal survival and growth (Wexler et al. 2011). The eggs hatched approximately 24 h after spawning and the yolk sac larvae were stocked at a density of 13 larvae L^{-1} (11,000 larvae) in each of three 828 L circular tanks. The seawater flow rate into each tank was maintained at 1.8 L min^{-1}, which resulted in three complete water exchanges per day. Four diffusers in each tank provided aeration according to standard protocols for each developmental stage (Margulies et al. 2016). Lights were set to a 12:12 light/dark cycle with stepped lighting during the first and last hours of the light cycle. Larvae from the three tanks were transferred at 13 dph to a larger, 1260-L-volume tank and water flow rates were increased to maintain approximately three complete water exchanges per day. Beginning at 2 dph, larvae were fed mean daily food levels of 2700–3600 enriched rotifers L^{-1} during the first 17 days of feeding: 1–22 copepods L^{-1} between 8 and 10 and between 21 and 23 dph, 50–208 enriched *Artemia* nauplii (Instar II stage) L^{-1} between 9 and 14 dph, and 7–28 yolk sac larvae L^{-1} between 14 and 25 dph. During feeding, a combination of *Nannochloropsis* sp. and *Thalassiosira* sp. algae was maintained in each tank at densities of approximately 1 million cells L^{-1}, which helped maintain prey quality and improve prey contrast to facilitate feeding.

Growth and development

Weighted exponential growth models were fitted to the SL and dry weight at age (x) data using Minitab® Inc. 2018 Statistical Software. Because the variances were not homogeneous, the inverse of the variance for SL and dry weight at age were used to calculate the weights in the models. Specific growth rates (SGR) as a percentage per day [$SGR = (e^b - 1) \times 100$] (Ricker 1975) were estimated for SL and dry weight using the weight- and length-specific growth coefficients (b) of the weighted exponential models. For larval SL, a total of 255 fishes were sampled: dph 2 = 25, dph 3 = 15, dph 4 = 15, dph 5 = 10, dph 6 = 10, dph 7 = 15, dph 8 = 15, dph 9 = 15, dph 10 = 10, dph 11 = 10, dph 12 = 15, dph 13 = 15, dph 14 = 15, dph 15 = 6, dph 16 = 5, dph 18 = 10, dph 22 = 10, dph 25 = 39. For larval weight, a total of 86 fishes were sampled: dph 2 = 14, dph 4 = 12, dph 9 = 15, dph 14 = 15, dph 18 = 10, dph 22 = 10, dph 25 = 10. Stages of morphological and physiological development of yellowfin tuna larvae were determined based on descriptions by Ambrose (1996) and Kaji et al. (1999).

Anti-NKA antibody

The α5 mouse monoclonal antibody used in this study was raised against the α-subunit of chicken NKA (Lebovitz et al. 1989, Developmental Studies Hybridoma Bank, Iowa City, IA, USA). This antibody specifically recognizes NKA α-subunits from multiple elasmobranch and teleost fishes including leopard shark (*Triakis semifasciata*; Roa et al. 2014; Roa and Tresguerres 2017), coho salmon (*Oncorhynchus kitsutch*; Wilson et al. 2002), blue-green damselfish (*Chromis viridis*; Tang et al. 2014), and giant mudskipper (*Periophthalmondon schlosseri*; Wilson et al. 2000), among others. We confirmed that the α5 antibody also recognizes the α-subunit of NKA in the yellowfin tuna (Supplementary material 2).

Immunohistochemistry

Beginning at the time of first feeding (2.2 dph), daily samples of 5–10 yellowfin larvae were collected, anesthetized with MS-222, and fixed in 3% paraformaldehyde, 0.35% glutaraldehyde, 0.1 M, pH 7.4 cacodylate buffer (cat# 15949 Electron Microscopy Sciences, Hatfield, PA, USA) for 6 h at 4 °C, 50% ethanol for 6 h at 4 °C, and then stored in 70% ethanol at 4 °C. For comparison with larval samples, gill samples from three sub-adult yellowfin tuna (54.9, 63.3, and 91.0 cm fork length) were collected by hook and line off the coast of San Diego, and fixed in 4% paraformaldehyde or 10% formalin buffered in seawater. Whole-mount immunohistochemical staining followed the protocol in Vectastain Ready-to-Use Kit (Vector Laboratories, Burlingame, USA) with some minor modifications. Fixed samples were treated with 3% hydrogen peroxide and tap water for 10 min, incubated in blocking buffer (normal horse serum) for 15 min, and incubated overnight with the anti-NKA antibody (1:1000 dilution in blocking buffer). The following day, samples were rinsed in phosphate buffered saline (3 × 10 min each) and incubated in pre-diluted biotinylated pan-specific secondary antibodies (Vector Laboratories) for 30 min. The samples were then rinsed and incubated in streptavidin/peroxidase reagent for 15 min. After rinsing, samples were stained with diaminobenzidine (DAB Peroxidase Substrate Kit; Vector Laboratories) according to the manufacturer's recommendations. A subset of samples was treated in an identical manner except that they were incubated in blocking buffer instead of primary antibody; these served as negative controls and had no specific staining.

Fluorescence immunohistochemistry followed protocols previously reported in Roa et al. (2014). The gills of fixed yellowfin tuna larvae were excised and consecutively

immersed in 95% ethanol (10 min), 100% ethanol (3 × 10 min), safeclear (3 × 10 min), and paraffin (55 °C) (3 × 30 min). Paraffin blocks solidified overnight and were cut into 10 µm sections using a rotary microtome. Three consecutive sections of each sample were placed on a slide and left in an incubator overnight (32 °C). Paraffin was removed in safeclear (10 min × 3), and rehydrated in 100%, 95%, 70% ethanol, and phosphate buffer saline (PBS; 10 min each). Slides were incubated in blocking buffer (PBS-Tx, 0.02% normal goat serum, 0.0002% keyhole limpet hemocyanin; 1 h), then incubated in the primary antibody (1:2000 in blocking buffer) overnight at RT. Slides were washed in PBS (10 min × 3), then incubated in goat anti-mouse Alexa Fluor™ 546 (ThermoFisher, Waltham, USA) secondary antibody (1:500, 1 h) and Hoechst 33342 (1:1000, 10 min) at RT. After they were washed again in PBS (10 min × 3), slides were mounted in Fluorogel with tris buffer (Electron Microscopy Sciences).

Light microscopy and imaging

Under the microscope, ionocytes were identified by their solid dark color resulting from intense NKA immunostaining. Yellowfin tuna larvae < 5 mm SL were examined using a Leica DMR compound microscope (Leica Microsystems, Inc., Buffalo Grove, IL, USA). Yellowfin tuna larvae > 5 mm SL were viewed with a Leica S8APO stereomicroscope. Images were captured with a Canon Rebel T3i SLR camera, z-stacked with Helicon Focus software (HeliconSoft, Kharkov, Ukraine), and stitched with Adobe Photoshop CS6 (Adobe Systems, San Jose, USA). All imaging on the skin was performed on the larva's right side. The gills and pseudobranch of yellowfin tuna larvae were also stained and studied. In this study, the term 'branchial' refers to both the pseudobranch and the gill. Branchial ionocytes were identified as explained above for the skin. All imaging of the branchial structures was performed on the larva's left side with its operculum pulled back.

Quantification of ionocyte number, size, density, and relative ionocyte area

After the images were processed as described above and counted by a researcher, ionocyte size and the larval surface area were traced with a stylus and measured through the freehand tool from the image analysis software Fiji (version 1.0; Schindelin et al. 2012).

Because NKA is present in the ionocyte basolateral membrane, the immunostained region is not on the skin surface. Therefore, the reporting of the percentage of "body surface occupied" by ionocytes (e.g., Varsamos et al. 2002a, b) based on NKA immunostaining is not technically correct. Instead, "relative ionocyte area" was calculated as the number of cutaneous ionocytes multiplied by their average area, then divided by the skin surface area. This parameter is a proxy for cutaneous ionocyte ion transporting capacity in relation to diffusional ion movement across the skin.

In larvae < 5 mm SL, all cutaneous ionocytes were counted and the skin surface area was measured using Fiji. In larger fish, the total number of cutaneous ionocytes was estimated by extrapolating counts from 10% of the total skin surface area by overlaying the sample's surface area with square coordinates, with each square's side corresponding to 2% of the larva SL (Supplementary Material 3). To account for potential differences in cell densities in the head, trunk, and fins, the number of squares sampled from each region was proportional to the surface area of each region. The squares were chosen by coding a random coordinate generator in R (ver. 0.98.1103), but discarded if (1) a square contained skin area from more than one region; (2) it contained glare, blank space (background beyond edge of fish), or pigment cells (which made it difficult to accurately identify all nearby ionocytes); (3) it contained area from the eye. The pectoral fin was removed and separately imaged and measured because it partially overlaps with the larvae's body. The first dorsal fin was excluded in the analysis because it is retractable and heavily pigmented, which prevented accurate measurements. To validate this sampling technique, the estimated number of cutaneous ionocytes was compared to the actual number counted throughout the entire skin for four larvae of different sizes (5.2, 8.8, 11.4, and 13.7 mm SL). The difference between the estimated and actual number of cutaneous ionocytes was 5.1 ± 0.5%.

Scanning electron microscopy

Yellowfin tuna samples were imaged using scanning electron microscopy (SEM) following protocols described in Wegner et al. (2013). Briefly, fixed samples were dehydrated to 100% tert-butyl alcohol in 25% increments over 24 h, frozen in 100% tert-butyl alcohol at 4 °C, and freeze dried using a VirTis benchtop freeze dryer (SP Industries, Gardiner, New York). Samples were then sputter-coated with gold and viewed using a FEI Quanta 600 SEM (FEI, Hillsboro, OR) under high-vacuum mode.

Statistics

Normalized ionocyte density across regions was analyzed with a one-way ANOVA ($\alpha = 0.05$), while ionocyte count and relative ionocyte area across development were fitted

with linear regressions using Graphpad Prism 6 (Graphpad, La Jolla, CA, USA).

Results

Growth and development

SL ($n = 255$) and dry weight ($n = 86$) increased exponentially between 2 and 25 dph (Fig. 1). The SGRs and 95% confidence intervals for SL and dry weight were $8.7 \pm 0.20\%$ d^{-1} and $37.0 \pm 1.0\%$ d^{-1}, respectively. Yellowfin tuna larvae in this study were in preflexion stage at ≤5 mm SL, notochord flexion stage between 5 and 7 mm SL, postflexion stage between 7 and 14 mm SL, and transformation stage between 14 and 24.5 mm SL (Fig. 1).

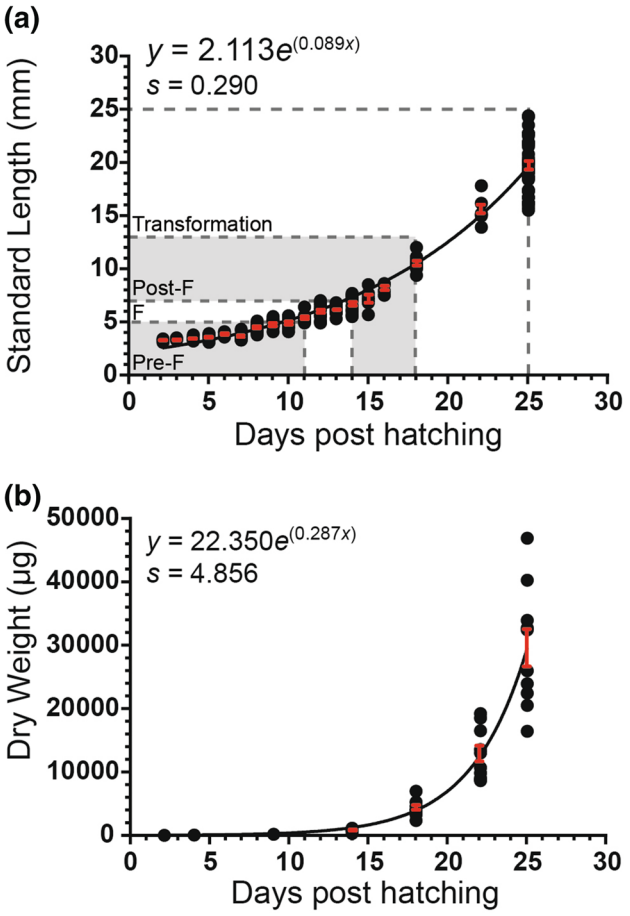

Fig. 1 Growth and development of yellowfin tuna larvae between 2 and 25 days post-hatching plotted against **a** standard length ($n = 255$) and **b** dry weight ($n = 86$), with their respective standard error bars (red error bars), non-linear regression equation, and standard error of the weighted exponential regression (s) fitted to the data. Dry weights were always > 0, but are below detection limits of scale for younger fish. *Pre-F* preflexion, *F* flexion, *Post-F* postflexion. (Color figure online)

Cutaneous ionocyte distribution throughout larval development

Yellowfin tuna larvae ($n = 18$) were selected to cover a range of SL between 2.9 and 24.5 mm throughout larval development. In the smallest larva (2.9 mm SL, 3 dph), ionocytes were predominately distributed along the head, pectoral fin, and anterior end of the trunk (Fig. 2a). Larvae in the flexion stage (~5–7 mm SL, 11–14 dph) additionally had ionocytes towards the end of the trunk, especially along the lateral midline and caudal fin rays (Fig. 2b). During the postflexion stage (7–14 mm SL, 14–18 dph), ionocytes were present throughout the body and concentrated on the head and along the lateral midline (Fig. 2c). Ionocytes were still present throughout the skin in the largest fish (24.5 mm SL, 25 dph) (Fig. 2d). There were no significant differences in normalized ionocyte densities between the head, trunk, and fins across development (ANOVA: $F_{2,42} = 0.8742$, $p = 0.4246$).

Cutaneous ionocyte number, size, density, and relative ionocyte area throughout larval development

The number of cutaneous ionocytes linearly increased with SL ($F_{1,16} = 146.8$, $p < 0.0001$; $r^2 = 0.9017$; Fig. 3a). Average cutaneous ionocyte size was ~300 µm^2 in 2.9 mm SL larvae, but it sharply decreased and plateaued at ~100 µm^2 in larvae 5 mm SL and larger (Figs. 2 insets and 3b). Cutaneous ionocyte density (number of cells per mm^2) had a biphasic pattern: it initially increased sharply, peaked at 5–7 mm SL, and then gradually decreased throughout the remainder of the development period examined (Fig. 3c). Relative ionocyte area decreased linearly with SL (linear regression: $F_{1,16} = 87.78$; $p < 0.001$; $r^2 = 0.8458$; Fig. 4a), with age (linear regression: $F_{1,16} = 38.85$; $p < 0.0001$; $r^2 = 0.7080$; Fig. 4b), and with accumulated thermal units (ATUs) (linear regression: $F_{1,16} = 42.54$; $p < 0.0001$; $r^2 = 0.7267$; Supplementary Material 4).

Branchial lamellae and ionocytes throughout larval development

Ionocytes were present in the gill arches in all examined larvae within the developmental time series examined (2.9–24.5 mm SL). Very small gill filaments and developing lamellae were detected as early as ~3.3 mm SL (4 dph); both were devoid of ionocytes (Fig. 5a, b). Ionocytes were first observed on the gill filament at 4.2 mm SL (7 dph; Fig. 5c, d). In post-flexion larvae (>7 mm SL; >14 dph), the gill filaments and lamellae continued to elongate and ionocytes remained present on the gill arch and filament (Fig. 5e, f). In the largest larva sampled (24.5 mm SL; 25 dph), the distal edges of adjacent gill lamellae began fusing together

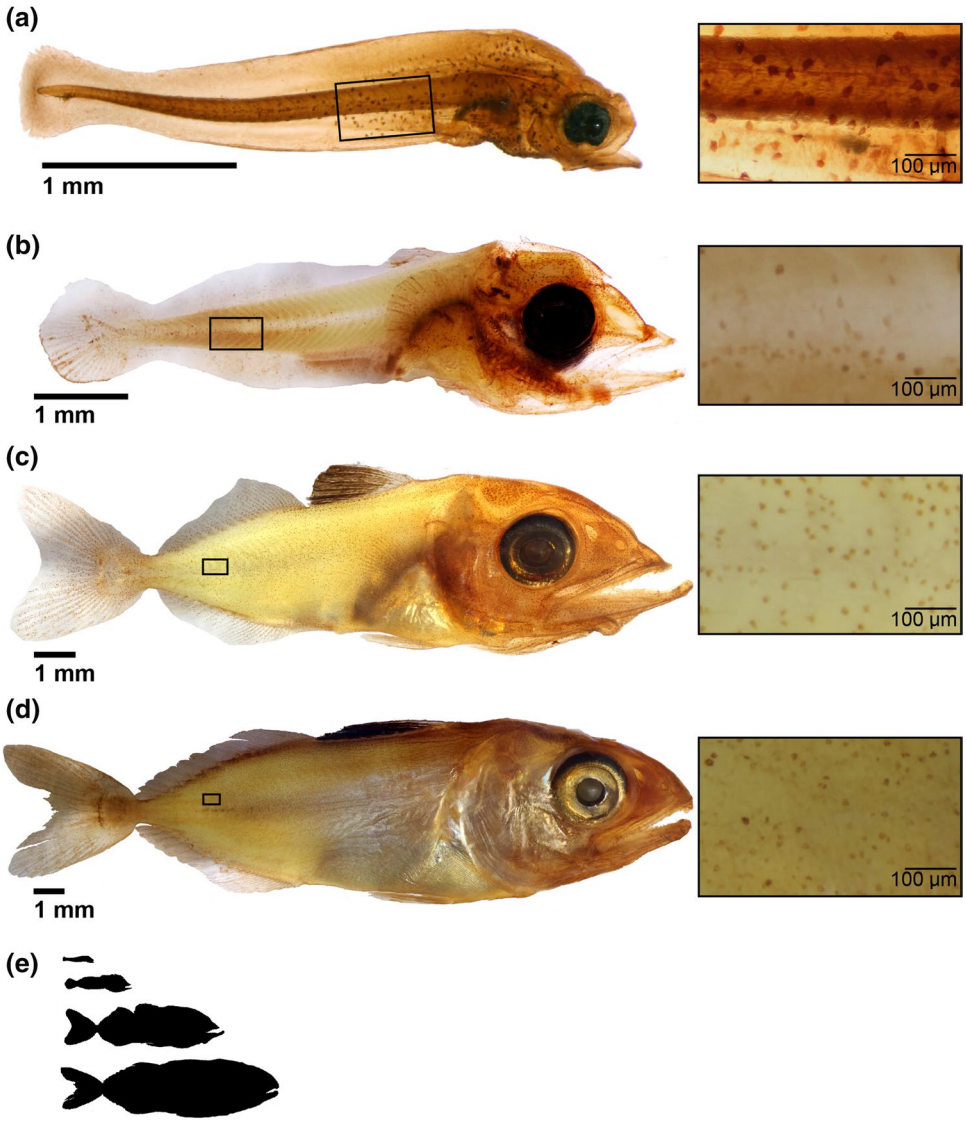

Fig. 2 Cutaneous ionocyte distribution across larval development in yellowfin tuna, with insets showing a magnified view of the ionocytes from each individual. **a** A 3.0 mm standard length (SL) larva showing ionocytes predominately on the head and the anterior region of the trunk. **b** Flexion larva (6.2 mm SL) showing cutaneous ionocytes beginning to appear on fin rays and throughout the trunk. **c** A 13.8 mm SL postflexion larva showing abundant cutaneous ionocytes still present throughout the body, particularly in the head and mid-lateral regions. **d** Cutaneous ionocytes in a 19.1 mm SL transformation-stage yellowfin. **e** Relative size comparison of the specimens shown in **a**–**d**

to form interlamellar fusions (Fig. 5g, h)—the precursor to complete lamellar fusions which develop later. Ionocytes were present along the interlamellar fusion (Fig. 5g, h), but were not observed on the actual gill lamellae of the larvae.

Pseudobranch lamellae were detected as early as ~3.3 mm SL (4 dph). In the pseudobranch, ionocytes were first observed in the filament and lamellae at ~3.4 mm SL (4 dph). Unlike the gills, pseudobranch ionocytes were present on both the filament and the lamellae throughout larval development, and adjacent pseudobranch lamellae did not fuse together in the size range examined (Fig. 6).

Ionocyte morphology throughout larval development

SEM imaging of larval yellowfin tuna skin and branchial structures ($n = 19$) identified three main epithelial cell types: pavement cells, mucous cells, and ionocytes. Pavement cells were characterized by their polygonal shape and array of microridges, while mucous cells had a smoothly-lined deep cavity from which mucus was often observed emerging. In the skin, there was a shift in ionocyte apical morphology around the flexion stage (~5–7 mm SL; 11–14 dph) from a wide area with extended microvilli (Fig. 7a) to pits (Fig. 7b). However, branchial ionocytes in both the pseudobranch (Fig. 6a, c) and the gills (Fig. 7c, d) had widened apical membranes with extended microvilli in all larval samples observed. Ionocytes on the fins had a wide and shallow apical membrane morphology (Fig. 7e, f).

Differential interference contrast (DIC) microscopy (also known as Nomarski interference contrast) overlaid with NKA immunofluorescence confirmed that the gill cells with wide apical membrane and extended microvilli were indeed ionocytes (Fig. 8).

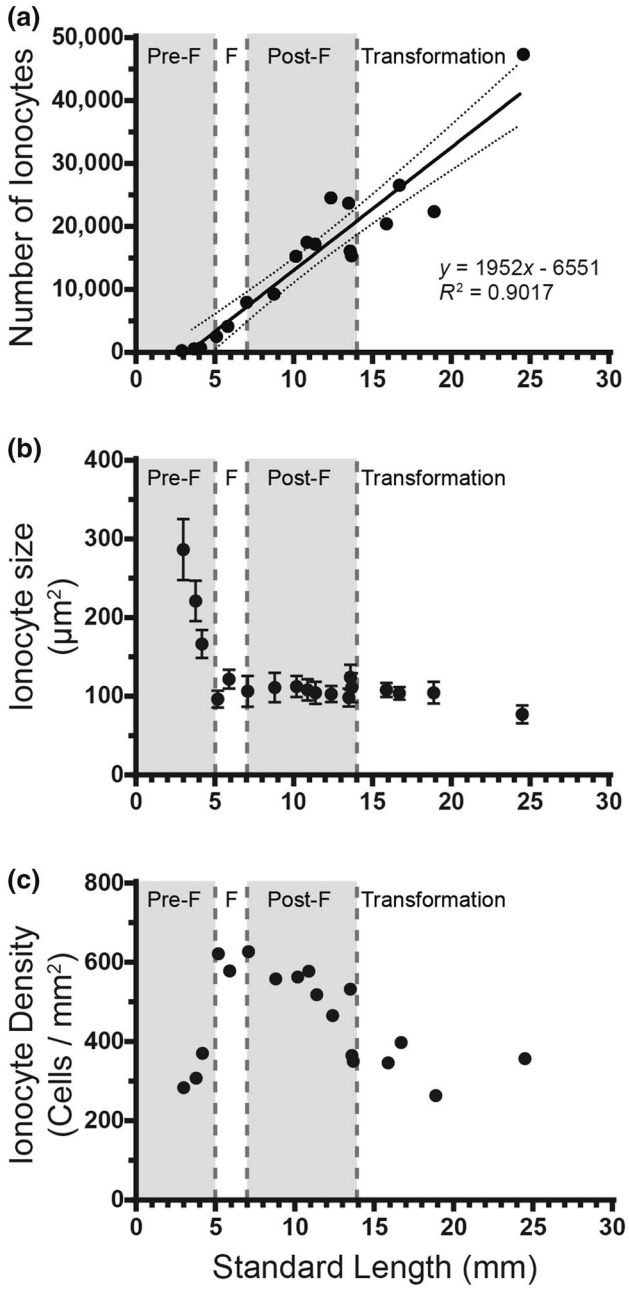

Fig. 3 Cutaneous ionocyte number (**a**), size (**b**), and density (**c**) in larval yellowfin tuna ($n=18$) ranging from 2.9 to 24.5 mm in standard length. Dotted lines in **a** denote 95% confidence levels. Error bars in **b** (gray) denote standard error of the mean. *Pre-F* preflexion, *F* flexion, *Post-F* postflexion

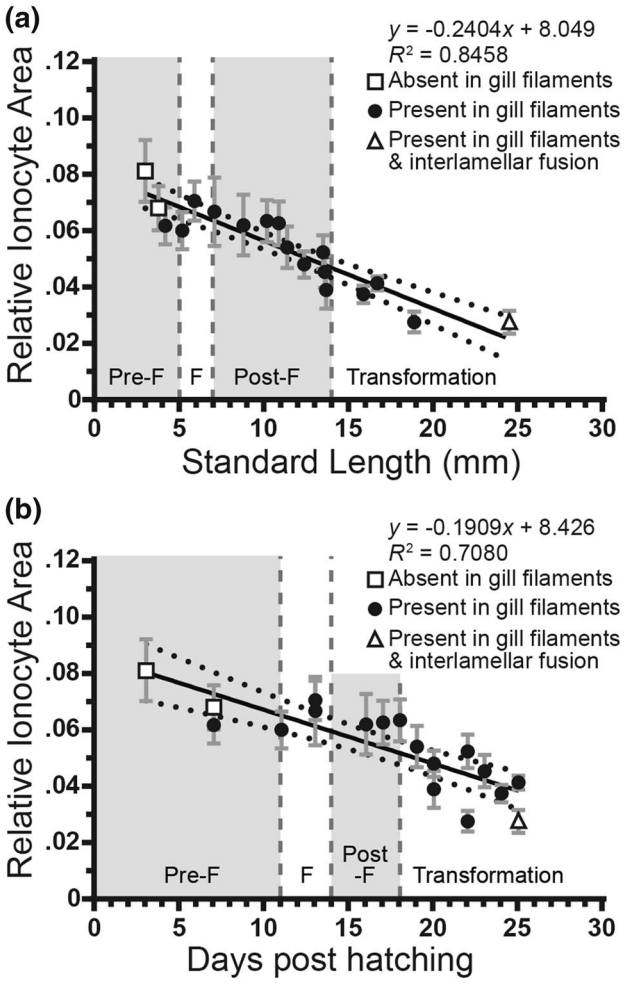

Fig. 4 Cutaneous ionocyte area relative to total skin surface area through larval yellowfin tuna development ($n=18$) in relation to **a** standard length (linear regression: $F_{1,16} = 87.78$; $p<0.001$; $r^2=0.8458$) and **b** days post-hatching (linear regression: $F_{1,16} = 38.80$; $p<0.0001$; $r^2=0.7080$). The black line shows the linear regression curve and dotted lines denote 95% confidence levels. Error bars (gray) denote standard error of the mean. Ionocyte absence in gills, presence in the gill filaments, and presence in interlamellar fusions and in the gill filaments is noted as a square, circle, and triangle, respectively. *Pre-F* preflexion, *F* flexion, *Post-F* postflexion

Gill ionocytes in sub-adult fish

The gills from sub-adult yellowfin tuna had ionocytes in the filaments and filament fusions (Fig. 9a), lamellar fusions (Fig. 9b), and also at the base of some lamellae. Ionocytes typically appeared retracted within apical pits (Fig. 9c, d).

Discussion

The survival pattern of the larvae reared for this study was typical of other yellowfin tuna cohorts raised in the laboratory from fertilized eggs where the majority of the mortality occurs during the first 10 days after hatching (Margulies et al. 2016). Larval metamorphosis was rapid and similar to previous studies (Ambrose 1996; Kaji et al. 1999; Margulies et al. 2016), and the variation and range in lengths increased with increasing dph (Fig. 1). This was likely due to different consumption, prey encounter, and metabolic rates. The gill morphology of the larger larvae within the same age group

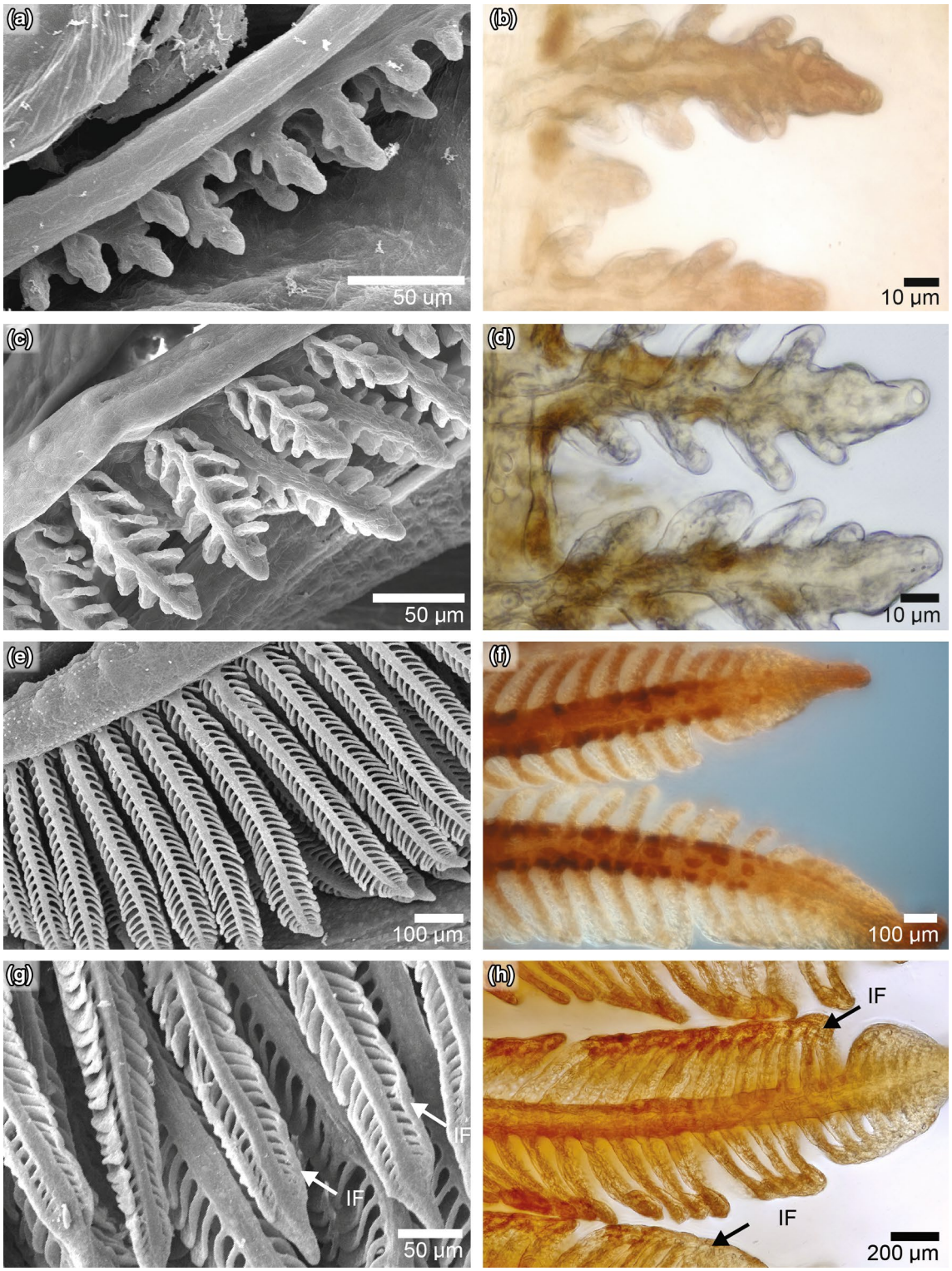

Fig. 5 Paired scanning electron micrographs **(a, c, e, g)** and Na^+/K^+ ATPase immunostained light microscopy images **(b, d, f, h)** showing the gill development and presence of ionocytes in a developmental time series of yellowfin tuna larvae. **a** Newly budding gills from a 3.3 mm standard length (SL) (4 dph) larva. **b** Absence of ionocytes in the gills of a 3.8 mm SL (6 dph) larva. **c** Further developed and defined filaments and lamellae in a 6.5 mm SL (15 dph) larva. **d** Strongly stained ionocytes in the gill filaments of a 4.2 mm SL (7 dph) larva. **e** The gill filaments and lamellae of a 15.4 mm SL (18 dph) larva. **f** Ionocytes in the gill filaments of a 16.7 mm SL (24 dph) larva. **g** Gills of a 20.5 mm SL (24 dph) transformation-stage larva showing the initial formation of interlamellar fusions binding adjacent lamellae near the filament tip. **h** Ionocytes on the gill filament and in the interlamellar fusions of a 24.5 mm SL (25 dph) yellowfin. Interlamellar fusions (IF) are indicated by arrows

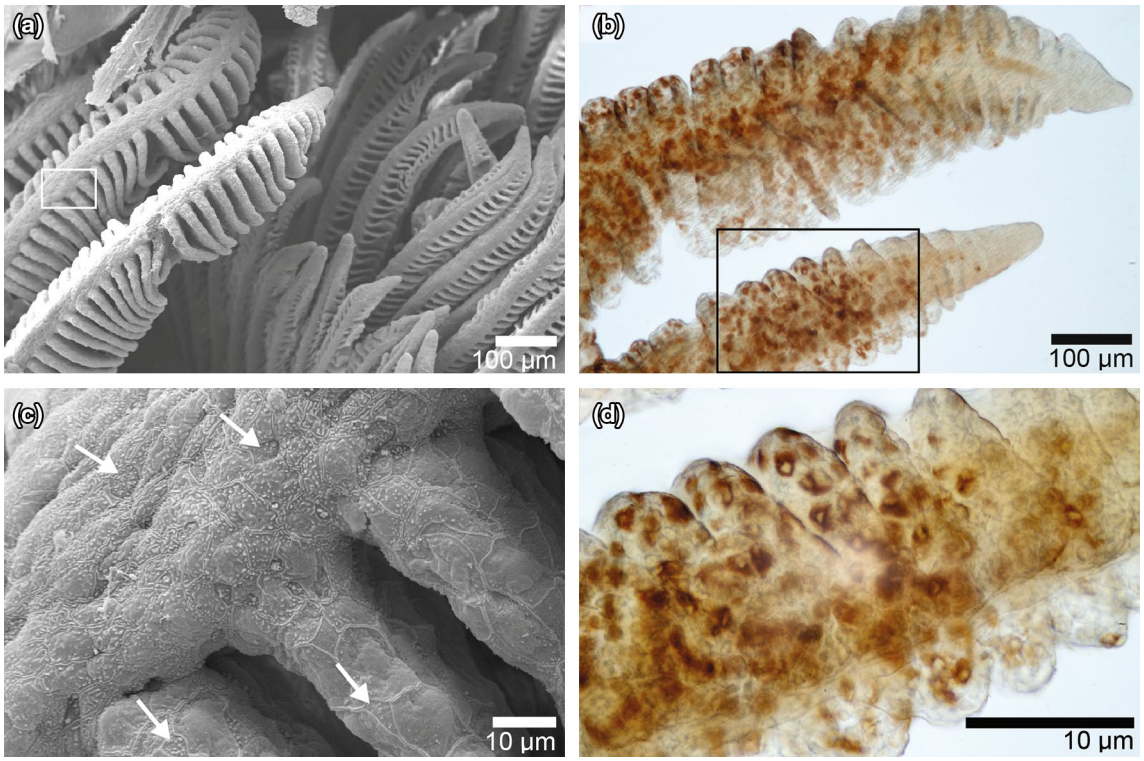

Fig. 6 Scanning electron **(a, c)** and light microscopy images **(b, d)** showing the presence of ionocytes on the filaments and lamellae of the pseudobranch of 18 mm standard length (SL) (25 dph) (**a, c**) and 19.6 mm SL (25 dph) transformation-stage yellowfin larvae (**b, d**). In **a** pseudobranch filaments are shown in the left foreground with gill filaments shown in the background (right). **c, d** are magnified views of the boxes shown in **a, b**, respectively. White arrows in **c** show the exposed apical surface of ionocytes on both the filament and lamellae of the pseudobranch

was more developed and indicated a more advanced stage in the transition from cutaneous to branchial gas exchange. This was especially evident at 25 dph larvae (672.38 ATU), where we did not observe interlamellar fusions in the smaller larvae (16.7 mm SL), but did so in the larger larvae (24.5 mm SL). These factors should be considered in future comparative studies of physiological and morphological development of yellowfin tuna larvae.

During the flexion stage, yellowfin tuna larvae have increased metabolic demands due to increasing ossification and chondrification and the rapid development of the digestive, neurological, and sensory systems (Richards and Dove 1971; Tanaka et al. 1996; Margulies 1997; Kaji et al. 1999). The increased development of the pseudobranch and gills as well as the transition from cutaneous to branchial gas exchange and osmoregulation also appear to take place around the flexion stage. In young larvae (< ~ 3.3 ml SL), the majority of gas exchange and osmoregulatory ion transport takes place across the skin. This is possible due to the large surface area to volume ratio of the larvae and the presence of abundant skin ionocytes (c.f. Goss et al. 1994; Perry and Goss 1994; Varsamos et al. 2002a; Katoh et al. 2003). As larvae grow larger (> ~ 3.3 ml SL), the pseudobranch and gills provide additional respiratory and osmoregulatory surface area to compensate for the decreased surface area to volume ratio and to keep up with increased metabolic rate. Although the total number of cutaneous ionocytes linearly increased throughout development, ionocyte size became smaller around the flexion stage—resulting in a linear decrease in relative ionocyte area and therefore active ion exchange capacity on the skin. This shift in ionocyte localization closely parallels previous studies in other marine teleosts, including larval Japanese flounder (*Paralichthys olivaceus*), killifish (*Fundulus heteroclitus*), European seabass (*Dicentrarchus labrax*), and gilthead sea bream (*Sparus aurata*) (Hiroi et al. 1998; Katoh et al. 2000; Varsamos et al. 2002a; Bodinier et al. 2010). Altogether, this indicates a shift in cutaneous to branchial osmoregulation around the flexion stage.

The apical morphology of cutaneous ionocytes also changed dramatically around the flexion stage, switching from a wide opening with extended microvilli in preflexion larvae to a pit in post-flexion larvae. During this transition, the number of branchial ionocytes progressively increased, and these ionocytes always had a wide apical opening with extended microvilli. The most extensively studied and

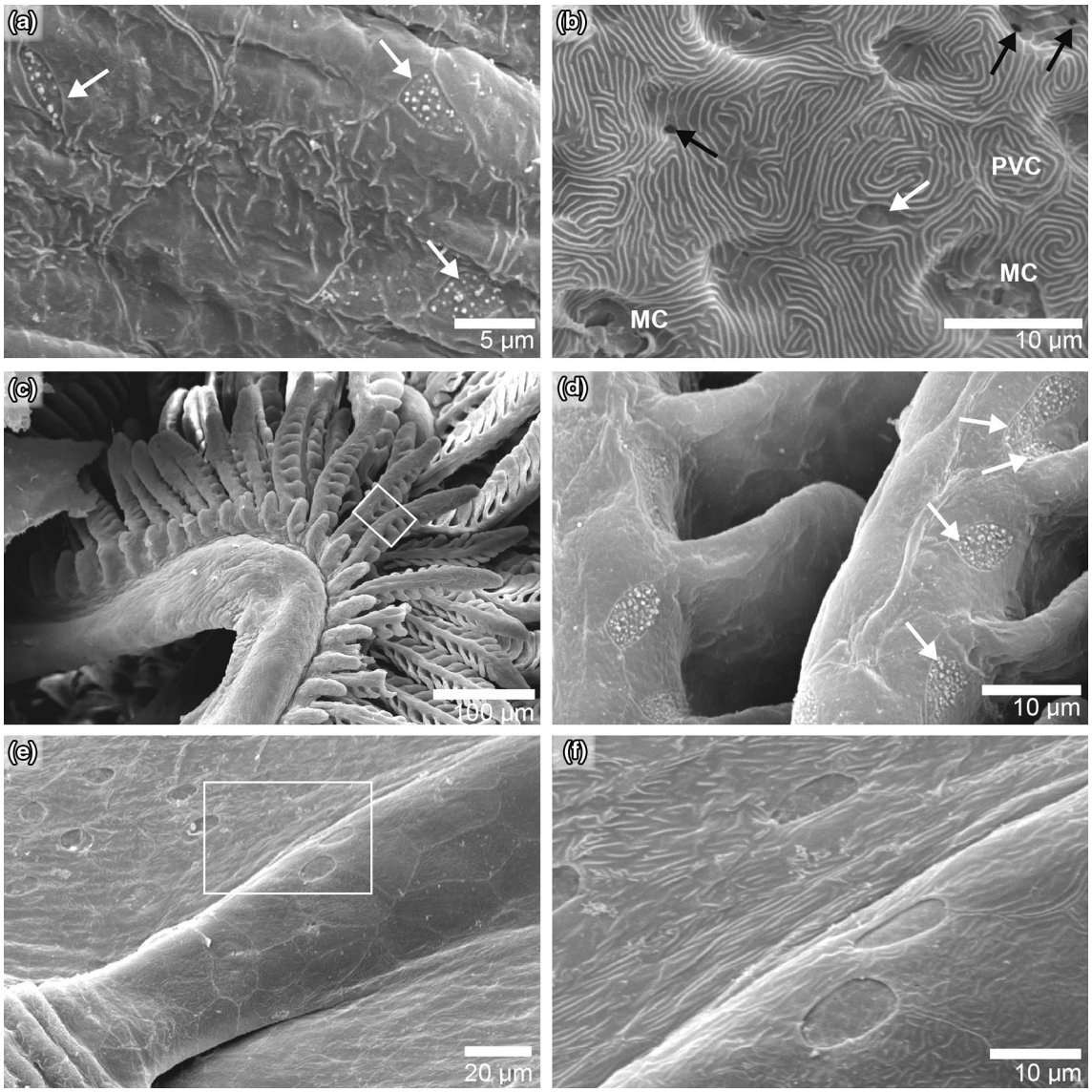

Fig. 7 Scanning electron micrographs of yellowfin tuna skin, gills, and dorsal fin. **a** Cutaneous ionocytes in a 3.8 mm standard length (SL), (10 dph) larva showing their exposed apical surfaces and protruding micovilli prior to the appearance of ionocytes in the gills. **b** Cutaneous ionocytes in a 6.5 mm SL (16 dph) larva, after the appearance of branchial ionocytes. **c** Gill arches, filaments, and lamellae from a 9.9 mm (20 dph) larva. **d** Higher magnification image of the white box shown in **c** showing gill filament ionocytes with exposed apical microvilli. **e** Second dorsal fin of a 9.9 mm SL (20 dph) larva showing the presence of ionocytes. **f** Higher magnification image of the white box in **e** showing dorsal fin ionocytes having a large exposed apical area that lacks extended microvilli. *PVC* pavement cell, *MC* mucous cells, black arrow ionocyte in apical pit; white arrow ionocyte with extended apical microvilli

reported ionocyte apical morphology is in the form of an apical pit (reviewed in Evans et al. 2005). However, a variety of ionocyte apical morphologies have been reported in gills from marine fish, including different degrees of exposure of the apical surface and microvilli (Laurent and Hebibi 1989; Franklin 1990; King and Hossler 1991; Brown 1992; Varsamos et al. 2002b). The exposure of gill ionocytes from European sea bass to doubly concentrated seawater showed that they undergo significant morphofunctional changes that include increased exposed apical surface area and NKA abundance (Varsamos et al. 2002b). Because survival in doubly concentrated seawater requires more active hypo-osmotic regulation, this ionocyte apical morphology has been linked to increased rates of NaCl excretion (Varsamos et al. 2002b). Based on that model, the change in apical morphology of cutaneous ionocytes of yellowfin tuna larvae during the flexion stage suggests downregulation, although not necessarily cessation, of NaCl excretion across the skin. Conversely, the exposed apical membrane and extended microvilli in branchial ionocytes of all larvae

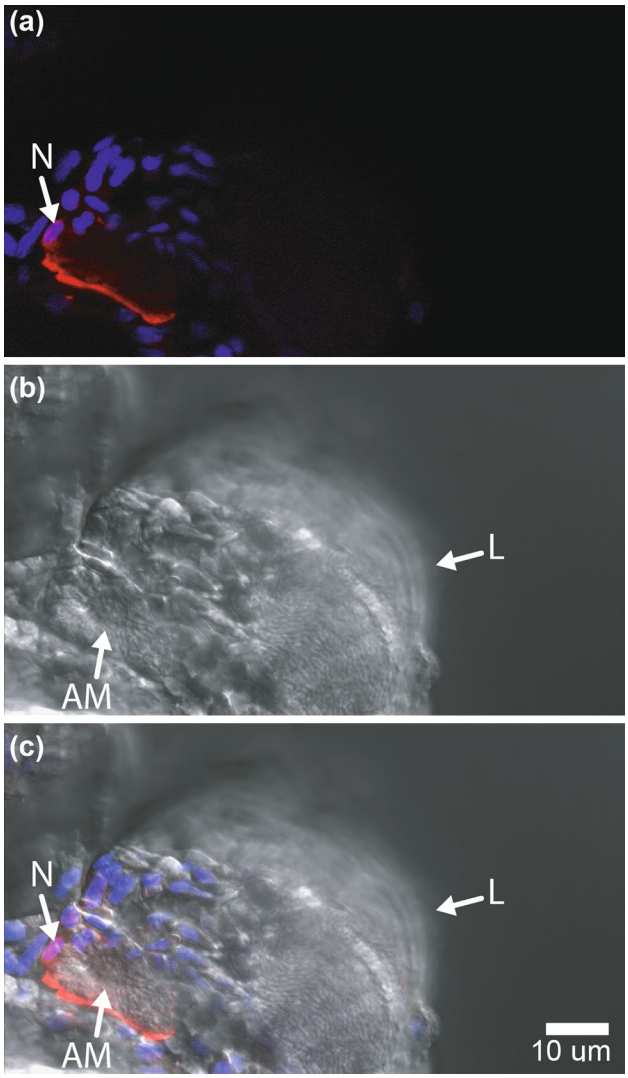

Fig. 8 Cross-section of an ionocyte on the gill filament of a post-flexion larval yellowfin tuna (12.2 mm SL; 24 dph). **a** Intense Na^+/K^+ ATPase signal was detected in the basolateral membrane of the ionocyte and **b** extended microvilli was observed in the widened apical pit of the ionocyte. The two images were merged in **c**. *N* nucleus of the ionocyte, *AM* apical membrane, *L* lamellae

that were examined suggest they were excreting NaCl at a high rate. However, only apical pits were observed in gills of the larger sub-adult yellowfin tuna examined which may reflect a decrease in mass-specific ionoregulation with growth as the fish surface area to volume ratio continues to decline. Altogether, our observations suggest covering and uncovering of the apical surface is a regulatory mechanism for ion transport in yellowfin tuna, similar to NaCl excretion in gills from European sea bass (Varsamos et al. 2002b) and to NaCl absorption in gills from freshwater teleosts (Goss et al. 1992a, b).

By the end of the transformation stage (~ 25 mm SL), branchial ionocytes also appeared along the gill interlamellar fusions, specialized gill structures found in some scombrids and billfishes that help the gills withstand the high-pressure ventilatory steam created by ram ventilation (Muir and Kendall 1968; Wegner et al. 2006, 2013). In yellowfin tuna, interlamellar fusions from adjacent filaments begin to merge together to form complete lamellar fusions starting about 3.2 cm FL (Wegner et al. 2013), and these are followed later by the development of filament fusions (Muir and Kendall 1968; Wegner et al. 2013). Examination of two larger yellowfin showed that ionocytes persist in these gill fusions as they grow. We hypothesize this novel ionocyte localization on the gill fusions is related to the need of yellowfin tuna (and presumably other scombrids and billfishes) for additional sites for ion regulation to maintain their large gill surface areas and a thin respiratory epithelial thickness (0.5–1.0 µm) required to meet their high metabolic demands (Hughes 1970; Wegner et al. 2006, 2010).

The physiological role(s) of the pseudobranch remains unclear (reviewed in Laurent and Dunel-Erb1984). In all larvae examined, the pseudobranch was extended within the buccal cavity and therefore exposed to environmental seawater. Furthermore, ionocytes developed on the pseudobranch filament and lamellae in high densities earlier than in the gill filaments, and remained abundant and with their apical surface exposed in the largest larvae (24.5 mm SL; 25 dph). These observations indicate the pseudobranch plays an important role in gas exchange and osmoregulation in developing yellowfin tuna larvae.

The yellowfin tuna larvae in the current study were raised in a land-based facility with optimal and near-constant salinity (~ 33 ppt), temperature (~ 28 °C), dissolved O_2 (~ 6 mg/L), and pH (~ 8.1) levels (Supplementary Material 1), which are representative of nearshore coastal conditions. However, the oceanic environment can be more variable. For example, yellowfin tuna spawn year-round off the coast of Costa Rica and Panama (Orange 1961; Schaefer 2001) where larvae are present at depths down to 50 m and may be exposed to seasonal changes in seawater salinity (28–35 ppt) and temperature (16–30 °C) (Lauth and Olson 1996; Owen 1997; Alory et al. 2012), and to changes in dissolved O_2 (2.0–7.3 mg/L) and pH (7.86–8.01) during upwelling events (Lauth and Olson 1996; Owen 1997; Rixen et al. 2012). In other teleosts, ionocytes have been shown to appear on the gill lamellae during hypo- (Uchida and Kaneko 1996; Sasai et al. 1998; Hirai et al. 1999; Zydlewski and McCormick 2001) and hyper-osmotic stress (Varsamos et al. 2002b), and upon experimentally induced decrease in temperature (Masroor et al. 2018), O_2 (Mitrovic et al. 2009), and pH levels (Leino and McCormick 1984). In addition, ionocyte distribution in marine teleost larvae may be affected by solar ultraviolet-B radiation (Sucré et al. 2012). If similar changes in ionocyte abundance and distribution occur in

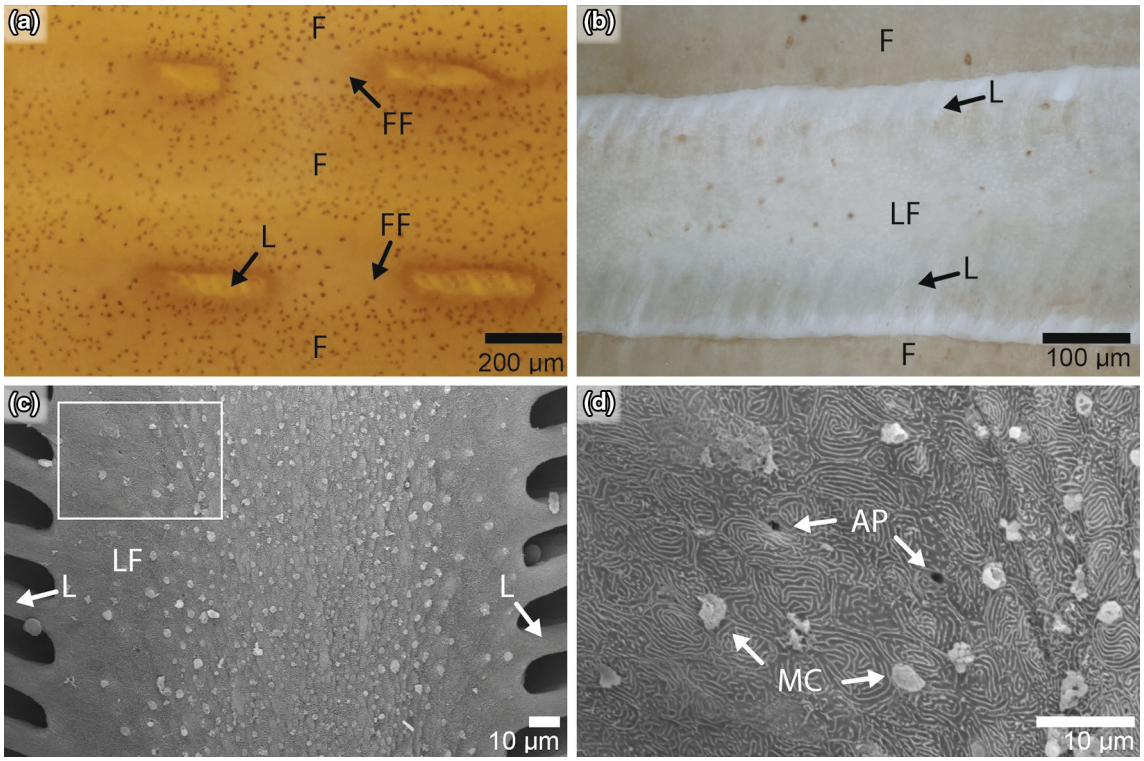

Fig. 9 Na^+/K^+ ATPase immunostained light microscopy images revealing ionocytes on the **a** filament, filament fusion, and **b** lamellar fusion of a sub-adult yellowfin tuna (54.9 cm fork length). **c** Scanning electron micrographs of ionocytes within the lamellar fusion of a sub-adult yellowfin tuna (91.0 cm fork length). **d** Higher magnification image of the white box in **c** showing lamellar fusion ionocytes in an apical pit. *FF* filament fusion, *F* filament, *L* lamella, *LF* lamellar fusion, *AP* apical pit, *MC* mucous cell

yellowfin tuna larvae exposed to changing environmental conditions, they would necessarily increase the thickness of the lamellar epithelium potentially affecting O_2 uptake. Such changes could compromise larval metabolic capacity, especially during the flexion stage.

In closing, this study provides a detailed description of the early development of gas exchange and osmoregulatory morphology of yellowfin tuna under optimum and constant rearing conditions. This information can be used as a baseline reference for studies of potential effects of environmental stressors on yellowfin tuna during early development in both aquaculture and the wild. Our study identified the flexion stage as a key transition point from cutaneous to branchial gas exchange and osmoregulation, the pseudobranch as a potentially important organ for gas exchange and osmoregulation during early development, and an unexpectedly complex apical ionocyte morphology. Finally, ionocytes were identified for the first time in interlamellar fusions of larval yellowfin tuna, and in the lamellar and filament fusions of larger individuals. Future in-depth studies should investigate whether morphological changes in ionocyte apical morphology is a regulatory mechanism for ion transport in marine fish, and its relevance for the physiology of fish living in a changing environment.

Acknowledgements This study was supported by the Inter-American Tropical Tuna Commission. We are grateful to the technical staff of the Achotines Laboratory in Panama for their assistance with measurements and larval rearing of yellowfin tuna. We thank Daniel Margulies and Vernon Scholey of the IATTC for development of yellowfin rearing methods and supervision of the spawning and larval rearing at the Achotines Laboratory. The authors would like to thank Dr. Greg Rouse for the use of microscope and camera equipment, Sabine Faulhaber for technical assistance with the scanning electron microscope, Taylor Smith for her assistance in dissection and imaging, and Johnathan Evanilla and Dan Fuller for providing sub-adult yellowfin tuna samples. We also thank William Watson (Southwest Fisheries Science Center) and Alex Da-Silva (Inter-American Tropical Tuna Commission) for helpful review comments. Lastly, we thank the editor and two anonymous reviewers for their helpful comments on an earlier draft. G.T.K. was supported by the San Diego Fellowship and the National Science Foundation Graduate Research Fellowship Program.

Compliance with ethical standards

Conflict of interest This study followed all applicable institutional guidelines for the care and use of animals. The authors declare they have no conflict of interest.

References

Alderdice DF (1988) Osmotic and ionic regulation in teleost eggs and larvae. In: Fish physiology. Academic Press, Cambridge, pp 163–251

Alory G, Maes C, Delcroix T, Reul N, Illig S (2012) Seasonal dynamics of sea surface salinity off Panama: the far eastern Pacific fresh pool. J Geophys Res Ocean 117:1–13. https://doi.org/10.1029/2011JC007802

Ambrose DA (1996) Scombridae: mackerels and tunas. In: Moser H (ed) The stages of fishes in the California current region, Calif. Coop. Ocean. Fish. Inves. Lawrence, Kansas, pp 1270–1285

Ayson FG, Kaneko T, Hasegawa S, Hirano T (1994) Development of mitochondrion-rich cells in the yolk-sac membrane of embryos and larvae of tilapia, *Oreochromis mossambicus*, in fresh water and seawater. J Exp Zool 270:129–135. https://doi.org/10.1002/jez.1402700202

Bodinier C, Sucré E, Lecurieux-Belfond L, Blondeau-Bidet E, Charmantier G (2010) Ontogeny of osmoregulation and salinity tolerance in the gilthead sea bream *Sparus aurata*. Comp Biochem Physiol A Mol Integr Physiol 157:220–228. https://doi.org/10.1016/j.cbpa.2010.06.185

Boehlert GW, Mundy BC (1994) Vertical and onshore-offshore distributional patterns of tuna larvae in relation to physical habitat features. Mar Ecol Prog Ser 107:1–13

Boehlert GW, Watson W, Sun LC (1992) Horizontal and vertical distributions of larval fishes around an isolated oceanic island in the tropical Pacific. Deep Res 39:439–466. https://doi.org/10.1016/0198-0149(92)90082-5

Brown P (1992) Gill chloride cell surface-area is greater in freshwater-adapted adult sea trout (*Salmo trutta*, L.) than those adapted to sea water. J Fish Biol 40:481–484. https://doi.org/10.1111/j.1095-8649.1992.tb02596.x

Brown CE, Muir BS (1970) Analysis of ram ventilation of fish gills with application to skipjack tuna (*Katsuwonus pelamis*). J Fish Res Board Can 27:1637–1652. https://doi.org/10.1139/f70-184

Evans DH (2002) Cell signaling and ion transport across the fish gill epithelium. J Exp Zool 293:336–347. https://doi.org/10.1002/jez.10128

Evans DH, Keys A (2008) Teleost fish osmoregulation: what have we learned since August Krogh, Homer Smith. AJP Regul Integr Comp Physiol 295:R704–R713. https://doi.org/10.1152/ajpregu.90337.2008

Evans D, Piermarini P, Potts W (1999) Ionic transport in the fish gill epithelium. J Exp Zool 283, 641–652. https://doi.org/10.1002/(SICI)1097-010X(19990601)283:7%3C641::AID-JEZ3%3E3.0.CO;2-W.

Evans DH, Piermarini PM, Choe KP (2005) The multifunctional fish gill: dominant site of gas exchange, osmoregulation, acid-base regulation, and excretion of nitrogenous waste. Physiol Rev 85:97–177. https://doi.org/10.1152/physrev.00050.2003

Franklin CE (1990) Surface ultrastructural changes in the gills of sockeye salmon (teleostei: *Oncorhynchus nerka*) during seawater transfer: comparison of successful and unsuccessful seawater adaptation. J Morphol 206:13–23. https://doi.org/10.1002/jmor.1052060103

Galland G, Rogers A, Nickson A (2016) Netting billions: a global valuation of tuna. Pew Charitible Trust, pp 1–22

Goss GG, Laurent P, Perry SF (1992a) Evidence for a morphological component in acid-base regulation during environmental hypercapnia in the brown bullhead (*Ictalurus nebulosus*). Cell Tissue Res 268:539–552. https://doi.org/10.1007/BF00319161

Goss GG, Perry SF, Wood CM, Laurent P (1992b) Mechanisms of ion and acid-base regulation at the gills of freshwater fish. J Exp Zool 263:143–159. https://doi.org/10.1002/jez.1402630205

Goss GG, Laurent P, Perry SF (1994) Gill morphology during hypercapnia in brown bullhead (*Ictalurus nebulosus*): role of chloride cells and pavement cells in acid-base regulation. J Fish Biol 45:705–718. https://doi.org/10.1111/j.1095-8649.1994.tb00938.x

Hirai N, Tagawa M, Kaneko T, Seikai T, Tanaka M (1999) Distributional changes in branchial chloride cells during freshwater adaptation in Japanese sea bass *Lateolabrax japonicus*. Zool Sci 16:43–49. https://doi.org/10.2108/zsj.16.43

Hiroi J, Kaneko T, Seikai T, Tanaka M (1998) Developmental sequence of chloride cells in the body skin and gills of Japanese flounder (*Paralichthys olivaceus*) larvae. Zool Sci 15:455–460

Hiroi J, Kaneko T, Tanaka M (1999) In vivo sequential changes in chloride cell morphology in the yolk-sac membrane of Mozambique tilapia (*Oreochromis mossambicus*) embyros and larvae during seawater adaptation. J Exp Biol 202:3485–3495

Hirose S, Kaneko T, Naito N, Takei Y (2003) Molecular biology of major components of chloride cells. Comp Biochem Physiol B Biochem Mol Biol 136:593–620. https://doi.org/10.1016/S1096-4959(03)00287-2

Holliday FGT (1969) The effects of salinity on the eggs and larvae of teleosts. In: Fish physiology. Academic Press, Cambridge, pp 293–311

Hughes GM (1970) Morphological measurements on the gills of fishes in relation to their respiratory function. Folia Morph 18:78–95

Kaji T, Tanaka M, Oka M, Takeuchi H, Ohsumi S, Teruya K, Hirokawa J (1999) Growth and morphological development of laboratory-reared Yellowfin Tuna *Thunnus albacares* and early juveniles, with special emphasis on the digestive system. Fish Sci 65, 700–707. https://doi.org/10.2331/fishsci.65.700

Katoh F, Shimizu A, Uchida K, Kaneko T (2000) Shift of chloride cell distribution during early life stages in seawater-adapted killifish, *Fundulus heteroclitus*. Zool Sci 17:11–18. https://doi.org/10.2108/zsj.17.11

Katoh F, Hyodo S, Kaneko T (2003) Vacuolar-type proton pump in the basolateral plasma membrane energizes ion uptake in branchial mitochondria-rich cells of killifish *Fundulus heteroclitus*, adapted to a low ion environment. J Exp Biol 206:793–803. https://doi.org/10.1242/jeb.00159

King JAC, Hossler FE (1991) The gill arch of the striped bass (*Morone saxatilis*). IV. Alterations in the ultrastructure of chloride cell apical crypts and chloride efflux following exposure to seawater. J Morphol 209:165–176. https://doi.org/10.1002/jmor.1052090204

Laurent P, Dunel-Erb S (1984) The pseudobranch: morphology and function. In: Hoar WS, Randall DJ (ed) Gills. Academic Press, Cambridge, pp 285–323

Laurent P, Hebibi N (1989) Gill morphometry and fish osmoregulation. Can J Zool 67:3055–3063. https://doi.org/10.1139/z89-429

Lauth RR, Olson RJ (1996) Distribution and abundance of larval Scombridae in relation to the physical environment in the northwestern Panama Bight. InterAm Trop TunaComm Bull 21:127–167

Lebovitz RM, Takeyasu K, Fambrough DM (1989) Molecular characterization and expression of the (Na++ K+)-ATPase alpha-subunit in *Drosophila melanogaster*. EMBO J 8:193–202

Leino RL, McCormick JH (1984) Morphological and morphometrical changes in chloride cells of the gills of *Pimephales promelas* after chronic exposure to acid water. Cell Tissue Res 236:121–128. https://doi.org/10.1007/bf00216521

Leis JM, Trnski T, Vivien MH-, Renon J, Dufour V, Moudni KE, Galzin R (1991) High concentrations of tuna larvae (Pisces: Scombridae) in near-reef waters of French Polynesia (Society and Tuamotu Islands). Bull Mar Sci 48:150–158

Margulies D (1997) Development of the visual system and inferred performance capabilities of larval and early juvenile scombrids. Mar Freshw Behav Physiol 30:75–98. https://doi.org/10.1080/10236249709379018

Margulies D, Wexler JB, Bentler KT, Suter JM, Masuma S, Tezuka N, Teruya K, Oka M, Kanematsu M, Nikaido H (2001) Early life history studies of Yellowfin tuna, *Thunnus albacares*. InterAm Trop Tuna Comm Bull 22:9–20

Margulies D, Suter JM, Hunt SL, Olson RJ, Scholey VP, Wexler JB, Nakazawa A (2007) Spawning and early development of captive Yellowfin Tuna (*Thunnus albacares*). Fish Bull 105:249–265

Margulies D, Scholey VP, Wexler JB, Stein MS (2016) Research on the reproductive biology and early life history of Yellowfin Tuna *Thunnus albacares* in Panama. In: Advances in Tuna Aquaculture: From Hatchery to Market. Elsevier, Amsterdam, pp 77–114

Marshall WS, Nishioka RS (1980) Relation of mitochondria-rich chloride cells to active chloride transport in the skin of a marine teleost. J Exp Zool 214:147–156. https://doi.org/10.1002/jez.1402140204

Masroor W, Farcy E, Gros R, Lorin-Nebel C (2018) Effect of combined stress (salinity and temperature) in European sea bass *Dicentrarchus labrax* osmoregulatory processes. Comp Biochem Physiol Part A 215:45–54. https://doi.org/10.1016/j.cbpa.2017.10.019

Mitrovic D, Dymowska A, Nilsson GE, Perry SF (2009) Physiological consequences of gill remodeling in goldfish (*Carassius auratus*) during exposure to long-term hypoxia. AJP Regul Integr Comp Physiol 297:R224–R234. https://doi.org/10.1152/ajpregu.00189.2009

Muir BS (1970) Contribution to the study of blood pathways in teleost gills. Copeia 1970:19 https://doi.org/10.2307/1441971

Muir BS, Brown CE (1971) Effects of blood pathway on the blood-pressure drop in fish gills, with special reference to tunas. J Fish Res Board Can 28:947–955. https://doi.org/10.1139/f71-140

Muir BS, Hughes GM (1969) Gill dimensions for three species of tunny. J Exp Biol 51:271–285

Muir BS, Kendall JI (1968) Structural modifications in the gills of tunas and some other oceanic fishes. Copeia 1968:388 https://doi.org/10.2307/1441767

Olson KR, Dewar H, Graham JB, Brill RW (2003) Vascular anatomy of the gills in a high energy demand teleost, the skipjack tuna (*Katsuwonus pelamis*). J Exp Zool 297A:17–31. https://doi.org/10.1002/jez.a.10262

Orange CJ (1961) Spawning of yellowfin tuna and skipjack in the eastern tropical Pacific, as inferred from studies of gonad development. InterAm Trop Tuna Comm Bull 5:459–526

Owen RW (1997) Oceanographic atlas of habitats of larval tunas in the Pacific Ocean off the Azuero Peninsula, Panama. InterAm Trop Tuna Comm Data Rep 9:1–32

Palzenberger M, Pohla H (1992) Gill surface area of water-breathing freshwater fish. Rev Fish Biol Fish 2:187–216. https://doi.org/10.1007/BF00045037

Perry SF, Goss GG (1994) The effects of experimentally altered gill chloride cell-surface area on acid-base regulation in rainbow trout during metabolic alkalosis. J Comp Physiol B Biochem Syst Environ Physiol 327–336 https://doi.org/10.1007/BF00346451

Richards WJ, Dove GR (1971) Internal development of young tunas of the genera Katsuwonus, Euthynnus, Auxis, and Thunnus (Pisces, Scombridae). Copeia 1971:72 https://doi.org/10.2307/1441600

Ricker W (1975) Computation and interpretation of biological statistics of fish populations. Bull Fish Res Board Can 191:382

Rixen T, Jiménez C, Cortés J (2012) Impact of upwelling events on the sea water carbonate chemistry and dissolved oxygen concentration in the Gulf of Papagayo (Culebra Bay), Costa Rica: implications for coral reefs. Rev Biol Trop 60:187–195

Roa JN, Munévar CL, Tresguerres M (2014) Feeding induces translocation of vacuolar proton ATPase and pendrin to the membrane of leopard shark (*Triakis semifasciata*) mitochondrion-rich gill cells. Comp Biochem Physiol Part A Mol Integr Physiol 174:29–37. https://doi.org/10.1016/j.cbpa.2014.04.003

Roberts J (1975) Active branchial and ram gill ventilation in fishes. Biol Bull 148:85–105

Roberts RJ, Bell M, Young H (1973) Studies on the skin of plaice (*Pleuronectes platessa* L.). II. The development of larval plaice skin. J Fish Biol 5:103–108. https://doi.org/10.1111/j.1095-8649.1973.tb04435.x

Rombough P (2007) The functional ontogeny of the teleost gill: which comes first, gas or ion exchange? Comp Biochem Physiol A Mol Integr Physiol 148:732–742. https://doi.org/10.1016/j.cbpa.2007.03.007

Sasai S, Kaneko T, Hasegawa S, Tsukamoto K (1998) Morphological alteration in two types of gill chloride cells in Japanese eels (*Anguilla japonica*) during catadromous migration. Can J Zool 76:1480–1487. https://doi.org/10.1139/z98-072

Schaefer KM (2001) Reproductive biology of tunas. In: Block BA, Stevens ED (eds) Tuna: physiology, ecology, and evolution. Academic Press, San Diego, pp 225–270

Schindelin J, Arganda-Carreras I, Frise E, Kaynig V, Longair M, Pietzsch T, Preibisch S, Rueden C, Saalfeld S, Schmid B et al (2012) Fiji: an open-source platform for biological-image analysis. Nature Methods 9:676 https://doi.org/10.1038/nmeth.2019

Schreiber AM (2001) Metamorphosis and early larval development of the flatfishes (Pleuronectiformes): an osmoregulatory perspective. Comp Biochem Physiol B Biochem Mol Biol 129:587–595. https://doi.org/10.1016/S1096-4959(01)00346-3

Shelbourne JE (1957) Site of chloride regulation in marine fish larvæ. Nature 180:920–922. https://doi.org/10.1038/180920a0

Stevens E (1972) Some aspects of gas exchange in tuna. J Exp Biol 56:809–823

Stevens ED, Lightfoot EN (1986) Hydrodynamics of water flow in front of and through the gills of skipjack tuna. Comp Biochem Physiol Part A Physiol 83:255–259. https://doi.org/10.1016/0300-9629(86)90571-2

Sucré E, Vidussi F, Mostajir B, Charmantier G, Lorin-Nebel C (2012) Impact of ultraviolet-B radiation on planktonic fish larvae: alteration of the osmoregulatory function. Aquat Toxicol 109:194–201. https://doi.org/10.1016/j.aquatox.2011.09.020

Tanaka M, Kaji T, Nakamura Y, Takahashi Y (1996) Developmental strategy of scombrid larvae: high growth potential related to food habits and precocious digestive system development. In: Watanabe Y, Yamashita Y, Oozeki Y (eds) Survival strategies in early life stages of marine resources. A A. Balkema, Rotterdam, pp 125–139

Tang CH, Leu MY, Yang WK, Tsai SC (2014) Exploration of the mechanisms of protein quality control and osmoregulation in gills of *Chromis viridis* in response to reduced salinity. Fish Physiol Biochem 40:1533–1546. https://doi.org/10.1007/s10695-014-9946-3

Uchida K, Kaneko T (1996) Enhanced chloride cell turnover in the gills of Chum Salmon fry in seawater. Zool Sci 13:655–660. https://doi.org/10.2108/zsj.13.655

van der Heijden AJH, van der Meij JCA, Flik G, Wendelaar Bonga SE (1999) Ultrastructure and distribution dynamics of chloride cells in tilapia larvae in fresh water and sea water. Cell Tissue Res 297:119–130. https://doi.org/10.1007/s004410051339

Varsamos S, Connes R, Diaz JP, Charmantier G, Dicentrarchus L (2001) Ontogeny of osmoregulation in the European sea bass. Mar Biol 138:909–915. https://doi.org/10.1007/s002270000522

Varsamos S, Diaz J, Charmantier G, Blasco C, Connes R, Flik G (2002a) Location and morphology of chloride cells during the post-embryonic development of the European sea bass, *Dicentrarchus labrax*. Anat Embryol (Berl) 205:203–213. https://doi.org/10.1007/s00429-002-0231-3

Varsamos S, Diaz JP, Charmantier GUY, Flik G, Blasco C, Connes R (2002b) Branchial chloride cells in sea bass (*Dicentrarchus labrax*) adapted to fresh water, seawater, and doubly concentrated

Journal of Comparative Physiology B
https://doi.org/10.1007/s00360-018-1187-9

Supplementary Material

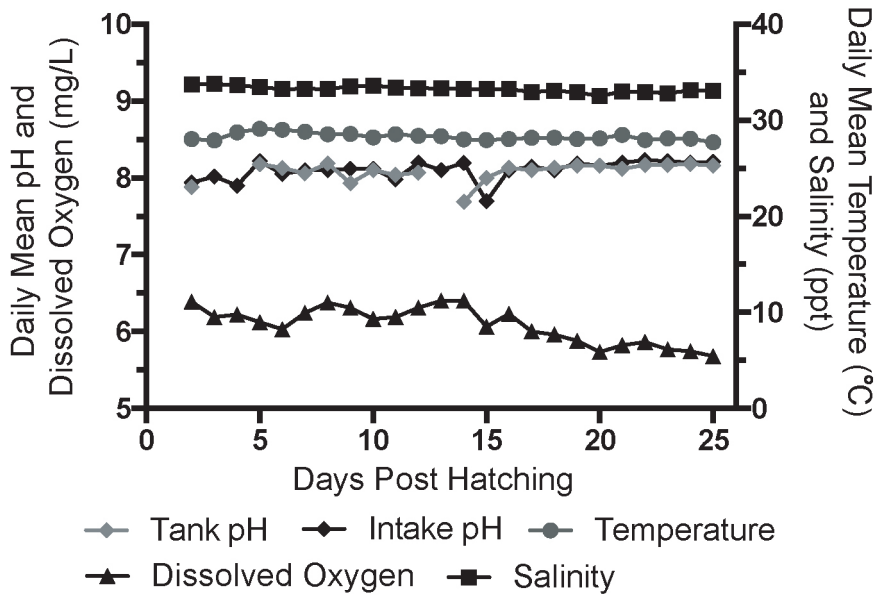

Supplementary material 1: Daily mean tank pH, intake pH, temperature (°C), dissolved O2 (mg/L), and salinity (ppt) throughout the yellowfin tuna larvae sampling period.

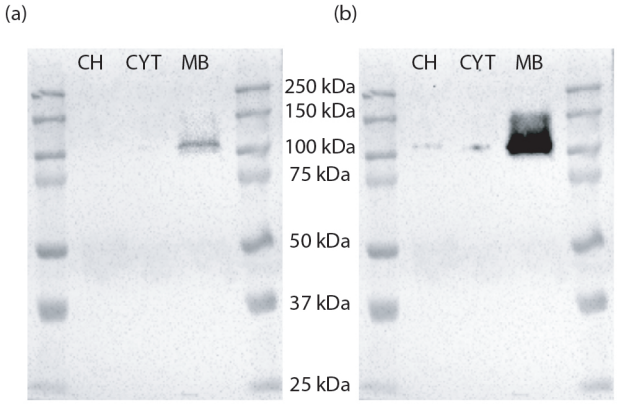

Supplementary material 2: Western blot with anti-Na+/K+-ATPase (NKA) monoclonal antibodies on sub-adult yellowfin tuna gill tissue yielded a single ~ 108 kDa band, which matches the predicted size of the protein. a NKA signal in the membrane fraction (MB) was significantly stronger (exposure time: 4 s) than b the crude homogenate (CH) and cytoplasm (CYT) fraction (exposure time: 304 s). This indicates NKA is present in the basolateral membrane as expected. Western blot method: gill samples were dissected from yellowfin tuna, immediately flash frozen in liquid N2, and kept at − 80 °C until processed. Frozen gill tissue was pulverized with porcelain mortar and pestle and mixed in an ice-cold protease inhibiting buffer (250 mmol L−1 sucrose, 1 mmol L−1 EDTA, 30 mmol L−1 Tris, 10 mmol L−1 benzamidine hydrochloride hydrate, 200 mmol L−1 phenylmethanesulfonyl fluoride, 1 mol L−1 dithiothreitol, pH 7.5). Debris was removed by low-speed centrifugation (3000×g for 10 min, 4 °C), and the resulting solution was saved as the crude homogenate fraction. A subset of the crude homogenate fraction was further subjected to a medium speed centrifugation (21130×g for 30 min, 4 °C), and the supernatant and membrane pellet was saved as the cytoplasmic fraction and the plasma membrane fraction, respectively. The total protein concentration of the three fractions was determined by Bradford protein assay, and 5 µg protein was combined with 2× Laemmli buffer (90%) and 2-mercapaethanol (10%). After heating at 70°C for 5 min, proteins were separated in 7.5% polyacrylamide mini gel (60 V 15 min, 200 V 45 min). Proteins were then transferred to a polyvinylidene difluoride (PVDF) membrane using a wet transfer cell (90 mA 8 h) (Bio-Rad, Hercules, CA, USA). After transfer, the PVDF membrane was incubated in blocking buffer (Tris-buffered saline, 1% tween, 10% skim milk) at room temperature (RT) for 1 h and incubated with the anti-NKA antibody (1.5 µg/mL) at 4 °C overnight. On the following day, the PVDF membrane was washed three times (10 min each) in Tris-buffered saline + 1% tween (TBS-T), incubated in goat anti-mouse HRP-linked secondary antibodies (1:10,000, Bio-Rad) at RT for 1 h and washed three times (10 min each) in TBS-T. Protein bands were made visible using ClarityTM Western ECL Substrate (Bio-Rad), and imaged and analyzed in a Bio-Rad Universal III Hood using ImageQuant software (Bio-Rad).

Published online: 24 October 2018

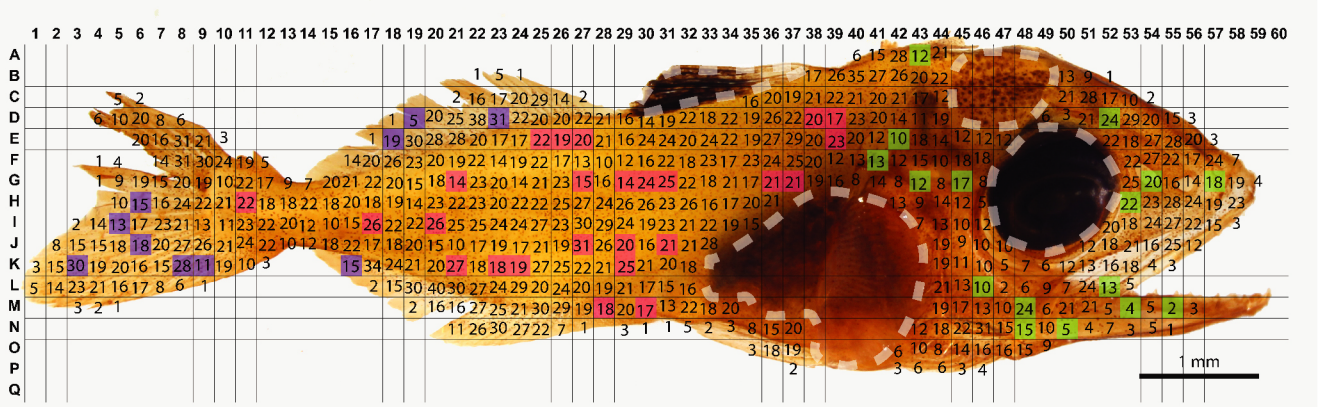

Supplementary material 3: Method for quantification of cutaneous ionocytes in yellowfin tuna larvae and early-stage juveniles >5 m SL. Ionocytes were identified by their intense Na+/K+-ATPase immunostaining and counted within randomly sampled boxes of the overlaid grid within the head (green), trunk (pink), and fin (blue) regions. Dashed white lines outline regions that were not sampled due to heavy pigmentation preventing accurate ionocyte counts .

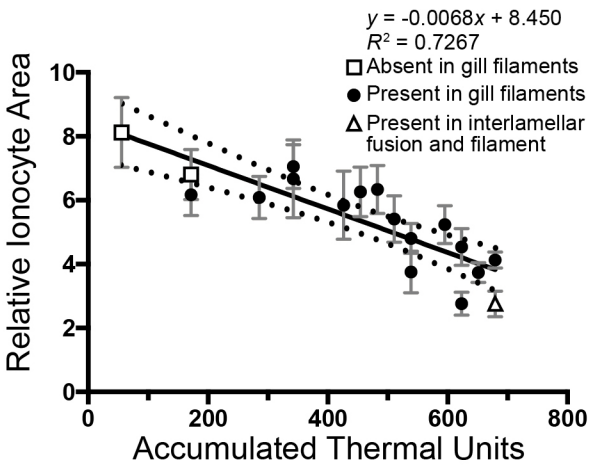

Supplementary material 4: Cutaneous ionocyte area relative to total skin surface area through larval yellowfin tuna development (n = 18) in relation to accumulated thermal units (linear regression: $F_{1,16} = 42.54$; $p < 0.001$; $r2 = 0.7267$). The black line shows the linear regression curve and dotted lines denote 95% confidence levels. Error bars (gray) denote standard error of the mean. Ionocyte absence in gills, presence in the gill filaments, and presence in interlamellar fusions and in the gill filaments is noted as a square, circle, and triangle, respectively.

Published online: 24 October 2018